

Discovery of a young asteroid cluster associated with P/2012 F5 (Gibbs)

Bojan Novaković^a Henry H. Hsieh^b Alberto Cellino^c

Marco Micheli^b Marco Pedani^d

^a*Department of Astronomy, Faculty of Mathematics, University of Belgrade, Studentski trg
16, 11000 Belgrade, Serbia*

^b*Institute for Astronomy, University of Hawaii, 2680 Woodlawn Drive, Honolulu, HI
96822, USA*

^c*INAF–Osservatorio Astrofisico di Torino, Via Osservatorio 20, I-10025 Pino Torinese,
Italy*

^d*Fundación Galileo Galilei - INAF Rambla José Ana Fernández Pérez, 7 38712 Breña
Baja, TF - Spain*

Abstract

We present the results of our search for a dynamical family around the active asteroid P/2012 F5 (Gibbs). By applying the hierarchical clustering method, we discover an extremely compact 9-body cluster associated with P/2012 F5. The statistical significance of this newly discovered Gibbs cluster is estimated to be $> 99.9\%$, strongly suggesting that its members share a common origin. The cluster is located in a dynamically cold region of the outer main-belt at a proper semi-major axis of ~ 3.005 AU, and all members are found to be dynamically stable over very long timescales. Backward numerical orbital integrations show that the age of the cluster is only 1.5 ± 0.1 Myr. Taxonomic classifications are unavailable for most of the cluster members, but SDSS spectrophotometry available for two cluster

members indicate that both appear to be Q -type objects. We also estimate a lower limit of the size of the parent body to be about 10 km, and find that the impact event which produced the Gibbs cluster is intermediate between a cratering and a catastrophic collision. In addition, we search for new main-belt comets in the region of the Gibbs cluster by observing seven asteroids either belonging to the cluster, or being very close in the space of orbital proper elements. However, we do not detect any convincing evidence of the presence of a tail or coma in any our targets. Finally, we obtain optical images of P/2012 F5, and find absolute R -band and V -band magnitudes of $H_R = 17.0 \pm 0.1$ mag and $H_V = 17.4 \pm 0.1$ mag, respectively, corresponding to an upper limit on the diameter of the P/2012 F5 nucleus of ~ 2 km.

Key words: Asteroids, dynamics; Comets; Photometry

1 Introduction

Asteroid families are believed to originate from catastrophic fragmentations of single parent bodies (Zappalà et al., 2002). They are very useful for studying various open problems in asteroid science (Cellino and Dell’Oro, 2010), and have been extensively investigated for almost a century. In principle, it is clear that “fresh” young families, only slightly evolved since the epoch of their formation, may provide more direct information about the collisional events from which they originated. In the last decade, our knowledge about such young families has been increased significantly. Several new ones have been discovered (e.g., Nesvorný et al., 2002, 2003, 2006; Nesvorný and Vokrouhlický, 2006; Nesvorný et al., 2008; Pravec and Vokrouhlický, 2009; Novaković, 2010; Vokrouhlický and Nesvorný, 2011; Novaković et al., 2012a,b), and many have been the subjects of detailed investigations (e.g., Vernazza et al.,

Email address: bojan@matf.bg.ac.rs (Bojan Novaković).

13 2006; Mothé-Diniz and Nesvorný, 2008; Takato, 2008; Vokrouhlický et al., 2009;
14 Cellino et al., 2010; Willman et al., 2010; Novaković et al., 2010; Ziffer et al., 2011).
15 Still, the search for new young families is very important in many respects. For in-
16 stance, there is a lack of young and dynamically stable groups belonging to the
17 taxonomic *C*-class, as was noted by Novaković et al. (2012b), who found the first
18 such example.

19 Another reason why young asteroid families are important is their likely relation
20 with a new class of asteroids identified in recent years, collectively known as *ac-*
21 *tive asteroids* (Jewitt, 2012). Active asteroids are objects which move along typical
22 asteroid orbits, but exhibit observable comet-like activity, i.e., mass loss, due to
23 one or more of different physical mechanisms as discussed by Jewitt (2012). The
24 two most plausible explanations for the activity observed for most active asteroids
25 are the sublimation of water ice and the impulsive ejection of material by an im-
26 pact. The main belt asteroids whose activity driver is most likely to be sublimation
27 are referred to as *main-belt comets* (MBCs; Hsieh and Jewitt, 2006). Objects dis-
28 playing likely impact-driven activity are known as *impacted asteroids* or *disrupted*
29 *asteroids*.

30 The existence of active asteroids, and MBCs in particular, challenges the traditional
31 view that asteroids and comets are two distinct populations, and supports asteroid-
32 comet continuum hypotheses (e.g., Gounelle et al., 2008; Briani et al., 2011). So
33 far, only a little more than a dozen active asteroids have been discovered, but their
34 number is constantly increasing with ongoing survey work (e.g., by the Catalina
35 Sky Survey, Pan-STARRS, and others) and the improvement of the telescopes, de-
36 tectors, and automated comet-detection algorithms used in such surveys.

37 The assumption that MBC activity is driven by volatile sublimation implies that

38 volatile compounds, i.e., ices, must be present on or immediately beneath the sur-
39 faces of these objects. It is difficult, however, to explain the survival of ices or other
40 volatiles on (or close to) the surfaces of objects orbiting at the heliocentric dis-
41 tances of the main asteroid belt over Gyr time-scales (Hsieh, 2009; Capria et al.,
42 2012). In fact, sublimation is expected to deplete the volatile content of the ex-
43 ternal layers of main belt objects over much shorter time scales. Hence, it has
44 been suggested that MBCs could be preferentially found among young asteroid
45 families, since the recently-formed members of these young families could still
46 retain significant reservoirs of volatile material immediately below their surfaces
47 which were previously deeply buried in the interior of the original parent bodies
48 (Nesvorný et al., 2008; Hsieh, 2009; Novaković et al., 2012a).

49 So far, links between MBCs and young families have been shown in only two
50 cases. 133P/Elst-Pizarro belongs to the young Beagle family, which is estimated
51 to be less than 10 Myr old (Nesvorný et al., 2008). The second example is that of
52 P/2006 VW₁₃₉, which is a member of a small cluster of objects estimated to be just
53 7.5 Myr old (Novaković et al., 2012a). If more cases of MBCs belonging to young
54 families can be found, it would lend strong support to the hypothesis that these fam-
55 ilies could preferentially contain more MBCs than the general asteroid population,
56 which could in turn lead to more efficient searches for even more MBCs and also
57 to greater insights into the physical conditions that give rise to MBC activity. Thus,
58 each time a new MBC is discovered, it is extremely important to check whether or
59 not an associated young asteroid family can be found.

60 Another reason why one could expect a cometary activity to be shared by different
61 members of a very young family is that a statistical analysis has shown the occur-
62 rence of a strong enhancement in the rate of mutual, low-energy collisions among
63 the members of newly-formed families (Dell’Oro et al., 2002). Although the pe-

64 riod during which the intra-member collision rate is enhanced over the background
65 collision rate is found to last only a relatively short time, and is expected to have
66 only a minimal effect on the long-term collisional evolution of the family, this ef-
67 fect could nonetheless have consequences on the cratering record on the surfaces
68 of family members, and could potentially enhance the likelihood of comet-like ac-
69 tivity arising on these objects.

70 Active asteroid P/2012 F5 (Gibbs) (hereafter P/2012 F5) was discovered last year
71 in Mt. Lemmon Survey data (Gibbs et al., 2012). To date, it has been the subject of
72 two published studies (Stevenson et al., 2012; Moreno et al., 2012), both suggest-
73 ing it is a disrupted asteroid, rather than a MBC. Before the origin of the activity of
74 P/2012 F5 had been conclusively determined, however, we had already begun the
75 search for a dynamical family associated with the object for the reasons described
76 above. We describe the results of that search in this paper.

77 The paper is organized as follows. First, in Section 2, we compute both the oscu-
78 lating and proper orbital elements of P/2012 F5. We then employ the hierarchical
79 clustering method to search for a family around P/2012 F5, successfully identify-
80 ing an associated young asteroid cluster that we have named the Gibbs cluster. In
81 Section 3, we determine the age of the Gibbs cluster, and in Section 4 we analyze
82 some of its physical properties. In Section 5, we present the results of an observa-
83 tional search for new MBCs in the region occupied by the cluster, and finally, in
84 Section 6, we discuss our results and conclusions.

85 **2 Search for a dynamical family associated with P/2012 F5 Gibbs**

86 *2.1 Determination of orbital elements*

87 To study the dynamical environment of P/2012 F5, we need reasonably good or-
88 bital elements for the object. This includes both osculating and proper elements.
89 However, shortly after its discovery, the orbit of P/2012 F5 was still characterized
90 by relatively large uncertainties. Thus, we made an effort to improve this situation
91 as much as possible.

92 For the purpose of orbit determination, we used three sets of astrometric obser-
93 vations collected over a period of ~ 3.6 years from 2009 September 17 to 2013
94 May 12. The largest portion of the dataset consists of 125 observations obtained
95 by various observing stations during the discovery apparition in 2012. In addi-
96 tion, 7 recovery observations were obtained by the authors in 2013 using the 3.6 m
97 Canada-France-Hawaii Telescope and the University of Hawaii 2.2 m telescope on
98 Mauna Kea. Finally, 17 precovery observations of this object were also found in
99 Pan-STARRS1 survey data, and were submitted to the Minor Planet Center by the
100 authors, adding an additional 2.4 years to the total observed arc for this object.

101 This total sample of 149 observations has been used in this work to carry out a
102 refined determination of P/2012 F5's orbit. The full dataset was first fit to a purely
103 gravitational orbit by weighting every observation according to the average histori-
104 cal performances of the observational station that obtained it. Gravitational pertur-
105 bations for all of the major planets and the three most massive main belt asteroids
106 were included in the computation. Astrometric residuals for each astrometric posi-
107 tion were then computed, and observations showing an offset in excess of $2''$ were

108 removed from the sample used to obtain the solution. A new orbit was then com-
109 puted, and this iterative process was repeated until a stable solution was achieved.
110 The final solution was found after rejecting 37 out of the 149 observations, where
111 all of the rejected observations were obtained in 2012 when the object was active.
112 The anomalous abundance of large outliers during this period is likely due to the
113 peculiar morphology of the object during its active phase, since the long tail struc-
114 ture and the lack of a clearly defined central condensation made it difficult to locate
115 the object’s photocenter (especially for small-aperture telescopes), in turn causing
116 a significant number of inaccurate positions to be reported to the Minor Planet
117 Center. In fact, among the rejected positions, some show astrometric residuals in
118 excess of 10 arcsec, mostly in the tail-ward direction. The resulting osculating or-
119 bit (Table 1) includes 112 positions, spanning an arc of 1333 days, and has an
120 RMS of about $0''.656$. The addition of non-gravitational terms following the usual
121 A1/A2 formalism does not improve the orbital fit, and no significant detection of
122 non-gravitational accelerations can therefore be extracted from this dataset.

123 Having obtained good osculating elements we can then proceed to the determina-
124 tion of proper orbital elements, which we did by applying the methodology de-
125 veloped by Milani and Knežević (1990, 1994). We compute P/2012 F5’s proper
126 semi-major axis (a_p), eccentricity (e_p), and inclination (i_p) and list their values in
127 Table 2.

128 2.2 *Application of the Hierarchical Clustering Method*

129 The next step in our study was to search for the presence of a dynamical asteroid
130 family around P/2012 F5. Families form dense clusters in the three-dimensional
131 space of proper semi-major axis (a_p), proper eccentricity (e_p), and proper inclina-

Table 1

The osculating orbit parameters and their corresponding formal errors at epoch JDT 2456400.5 (2013 Apr 18.0 TT) for active asteroid P/2012 F5.

Orbital element	Symbol	Value	Error	Units
Semi-major axis	a	3.0050440	9.78e-7	AU
Eccentricity	e	0.0417036	2.22e-7	-
Inclination	i	9.73869	0.000026	deg
Argument of perihelion	ω	177.82221	0.0007	deg
Longitude of node	Ω	216.85955	0.00012	deg
Mean anomaly	M	210.98151	0.0008	deg
Perihelion distance	q	2.87972262	1.21e-6	AU
Aphelion distance	Q	3.13036534	1.15e-6	AU
Perihelion passage	t_p	2457188.112002	0.00472	JD

132 tion (i_p), and can be identified by analyses of the distribution of objects in proper
 133 element space to search for such clusterings. In our analysis, we apply the hierar-
 134 chical clustering method (HCM) to perform this analysis and adopt the ‘standard’
 135 metric, d_c , proposed by (Zappalà et al., 1990, 1994).

136 The HCM identifies groupings of objects having mutual separations below a thresh-
 137 old ‘distance’ (d_c), which, adopting standard conventions, has units of m s^{-1} . We
 138 apply the HCM to a catalog of analytically-determined proper elements (Milani and Knežević,
 139 1990, 1994) available at the *AstDyS* web repository as of November 2012 (<http://hamilton.dm.unipi.it/astdys/>).
 140 Analytical proper elements are reasonably accurate for objects with low to moder-

141 ate orbital eccentricity and inclination. We use them because they are available for
142 both numbered and multi-opposition asteroids. The proper elements of P/2012 F5
143 that we obtained here are also added to the catalog.

144 We carry out our HCM analysis by testing a range of cutoff distances from 5 to
145 70 m s^{-1} and noting the number of asteroids that the analysis links to P/2012 F5 at
146 those separations. At the beginning of our search, we change d_c in discrete steps of 1
147 m s^{-1} , but after identifying the family at 7 m s^{-1} , we switch to steps of 5 m s^{-1} . Our
148 results are shown in Figure 1. We find that a cluster of asteroids around P/2012 F5
149 does indeed exist, and hereafter will refer to it as the Gibbs cluster¹. This cluster
150 is extremely compact and is clearly separated from background objects in proper
151 element space. Given how compact the core of the cluster is, we do not believe that
152 the asteroids associated with the cluster for $d_c > 40 \text{ m s}^{-1}$ are real members.

153 The structure of the cluster in the space of proper orbital elements is shown in
154 Figure 2. In this figure, all asteroids located in the region of the Gibbs cluster are
155 shown in two planes (semi-major axis vs. eccentricity and semi-major axis vs. sine
156 of inclination), and by using two different scales. In the plots, the superimposed
157 ellipses represent equivelocity curves, computed according to the Gauss equations
158 (Morbidelli et al., 1995). These ellipses are obtained assuming a velocity change
159 $\Delta v = 10 \text{ m s}^{-1}$, argument of perihelion $\omega = 90^\circ$, and true anomaly $f = 90^\circ$. The
160 ellipses are shown as an illustration of the limiting distance between the parent body
161 and the other fragments in the isotropic ejection field. However, the ejection field of
162 the Gibbs cluster is clearly asymmetric, a property that is usually interpreted as in-

¹ The usual practice is to name asteroid families after their lowest numbered member. However, for groups that are known to contain an active asteroid and that are discovered as the result of a search around that active asteroid, we have decided to name them after the member known to be active.

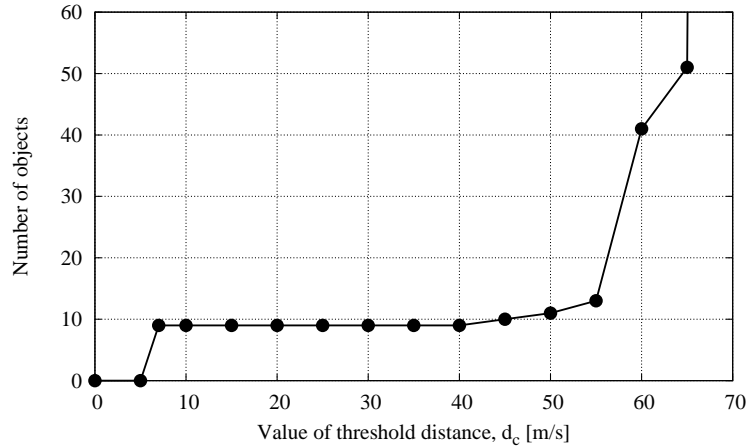


Fig. 1. Number of asteroids associated with P/2012 F5 as function of cut-off distance (in velocity space), expressed in m s^{-1} . The dominant feature is the existence of a small group consisting of nine members. These objects are very tightly packed in proper orbital element space.

163 dicating that a family is the result of a cratering event (Vokrouhlický and Nesvorný,
 164 2011; Novaković et al., 2012b).

165 2.3 Statistical significance of the cluster

166 An important additional step in any family identification analysis is evaluation of
 167 the statistical significance of any identified groups in order to avoid confusing true
 168 families (i.e., clusters of asteroids sharing a mutual collisional origin) with group-
 169 ings which are simply statistical flukes. To evaluate the significance of the Gibbs
 170 cluster, we first note that its members are extremely tightly packed in proper orbital
 171 element space. We further note that the density of asteroids in the immediate vicin-
 172 ity of the Gibbs cluster is relatively low. This can be seen by looking at the four
 173 plots shown in Figure 2. There are a few background asteroids located inside the
 174 equivelocity ellipses in one plot or another, but these are not the same objects in
 175 both planes. As such, none of these objects are actually located within the proper

Table 2

List of asteroids belonging to the Gibbs cluster.

Asteroid ^a	a_p ^b	e_p ^c	$\sin(i_p)$ ^d	H ^e	D_1 ^f	D_2 ^g	T_{lyap} ^h
20674	3.00423	0.02324	0.17974	12.6	17.9	9.0	0.65
140429	3.00381	0.02315	0.17972	15.0	5.9	3.0	3.33
177075	3.00509	0.02289	0.17973	15.6	4.5	2.3	0.63
249738	3.00481	0.02294	0.17971	15.7	4.3	2.2	0.68
257134	3.00514	0.02300	0.17970	15.8	4.1	2.1	0.67
321490	3.00514	0.02299	0.17971	15.8	4.1	2.1	0.65
2007 RT ₁₃₈	3.00484	0.02310	0.17969	15.7	4.3	2.2	0.65
2002 TF ₃₂₅	3.00503	0.02288	0.17968	17.1	2.3	1.1	0.67
P/2012 F5	3.00386	0.02274	0.17972	17.4	2.0	1.0	0.83

^a Asteroid number or provisional designation^b Proper semi-major axis in AU^c Proper eccentricity^d Sine of proper inclination^e Absolute magnitude^f Diameter in km, when an albedo of $p_v = 0.05$ is assumed^g Diameter in km, when an albedo of $p_v = 0.2$ is assumed^h Lyapunov time in Myr

¹⁷⁶ element space region defined by the cluster.

¹⁷⁷ Relatively close to the Gibbs cluster, there is the very large Eos family. This fam-
¹⁷⁸ ily is among the largest and oldest groups in the main belt (Vokrouhlický et al.,
¹⁷⁹ 2006). However, the eccentricities of asteroids belonging to the Gibbs cluster are
¹⁸⁰ substantially lower than those of Eos family members, even when a possible ex-

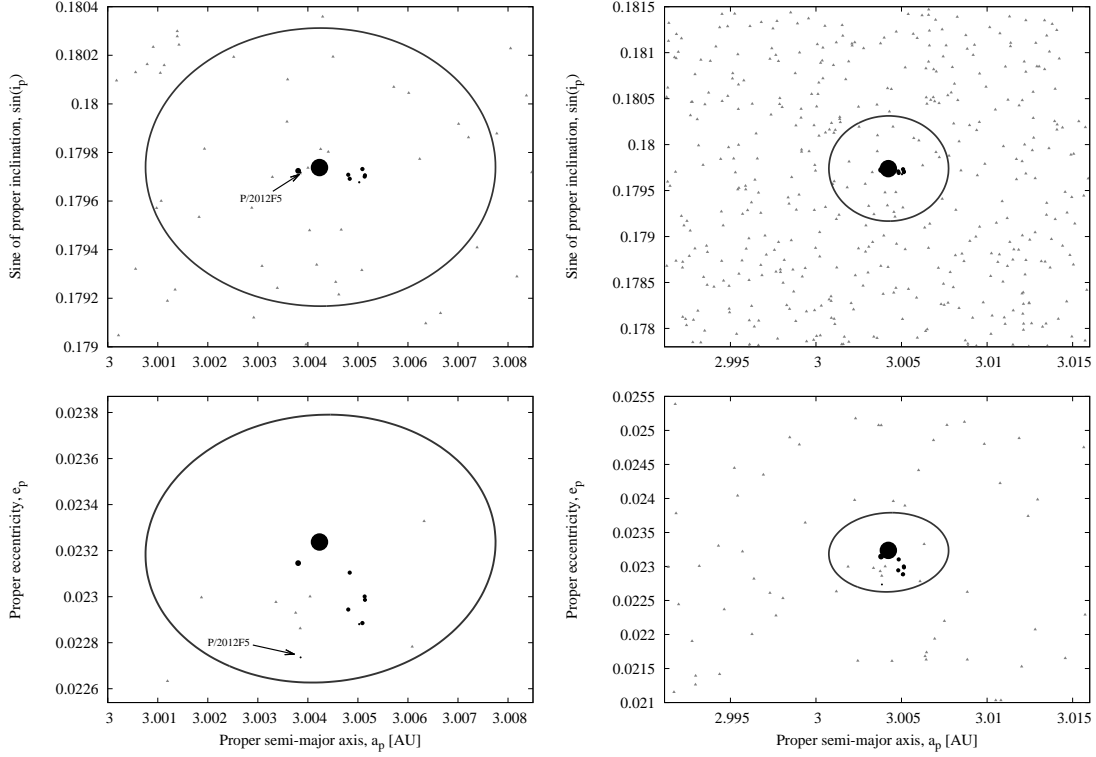


Fig. 2. The region of the main asteroid belt in which the Gibbs cluster is located. The plots represent the space of proper orbital elements, in two different planes (top/bottom) and scales (left/right). The members of the cluster are shown as black filled circles, and the size of their symbols is proportional to the corresponding diameter. Nearby background asteroids are shown as gray filled triangles. For the meaning of the elliptical curves, see the text.

181 ternal halo of Eos family members is considered (Brož and Morbidelli, 2013). We
 182 therefore consider the Gibbs cluster to be clearly separated from the Eos family,
 183 and likely completely unassociated with it. Moreover, the little spectroscopic data
 184 available for the Gibbs cluster also seem to rule out any relation with the Eos family
 185 (discussed below).

186 Nesvorný et al. (2002) furthermore showed that, even within the borders of the
 187 large and dense Koronis family, using a very low critical distance threshold for
 188 family identification of $d_c = 10 \text{ m s}^{-1}$, clusters of only up to 5 members could be

189 found by chance. This result suggests that a concentration of asteroids as tight and
190 dense as the Gibbs cluster is not easily achievable, even within very densely popu-
191 lated volumes of proper element space, including those occupied by extremely large
192 asteroid families like Eos, Themis and Koronis, further suggesting that the Gibbs
193 cluster is a true asteroid family, and not a statistical fluke, and that its members
194 share a common collisional origin.

195 To make a more quantitative assessment of the significance of the Gibbs cluster, we
196 also perform the following test. First, in the space of proper orbital elements, we
197 generate 1000 different synthetic main asteroid belts, each one including 336 555
198 fictitious objects drawn from a quasi-random distribution (QRD) fitting the distri-
199 butions of a_p , e_p , and $\sin(I_p)$ exhibited by the known asteroids in the real main
200 asteroid belt. By doing this, we are able to experiment with different random pop-
201 ulations while still taking into account the structure of the real asteroid belt. The
202 complete procedure to obtain the QRD is described in Novaković et al. (2011). We
203 then apply the HCM to each of our 1000 synthetic main belts. Using the cut-off
204 distance of 7 m s^{-1} (the level at which the Gibbs cluster is detected), we fail to
205 find any group with at least 9 members. We therefore conclude that the statistical
206 significance of the Gibbs cluster is $> 99.9\%$.

207 Despite the results presented above, one should keep in mind that the high statistical
208 significance of the cluster itself does not imply that there are no interlopers. A priori
209 we cannot exclude a possibility that any single member is an interloper.

210 **3 Age of the Gibbs cluster**

211 The most appropriate and accurate way to determine the age of a young family
212 is the so-called backward integration method (BIM; Nesvorný et al. (2002)) The
213 strategy behind the BIM relies on the fact that immediately after the disruption of
214 a parent body, the orbits of the fragments are nearly identical (being determined
215 by the ejection velocities through the Gauss equations), but then tend to diverge
216 as a function of time due to planetary perturbations and non-gravitational effects.
217 Consequently, two secular angles that determine the orientation of an orbit in space,
218 namely the longitude of the ascending node (Ω) and the argument of perihelion
219 (ω), for different objects evolve with different, but nearly constant, speeds. After
220 some time, this effect tends to spread out the distributions of Ω and ω of the family
221 members uniformly over 360° . Therefore, the age of a young asteroid family can
222 be determined by numerically integrating the orbits of its members backwards in
223 time until the orbital orientation angles cluster around single values. Of course, this
224 can be reliably done only when a family is sufficiently young that the dynamical
225 evolution of its members, following fragmentation of the parent body, has not yet
226 completely erased information about the primordial orbits.

227 This method, either in its original form or with some variations, has been used many
228 times in the last decade to estimate the age of young families. For example, the BIM
229 has been used to determine the ages of the Karin cluster (Nesvorný et al., 2002),
230 Veritas family (Nesvorný et al., 2003), Datura cluster (Nesvorný et al., 2006), Theobalda
231 family (Novaković, 2010), and Lorre cluster (Novaković et al., 2012b). Here, we
232 obtain the age of Gibbs cluster using two approaches based on the BIM. First, we
233 determine the cluster's age by numerically integrating the orbits of the nominal
234 cluster members, as originally proposed by Nesvorný et al. (2002). Second, we re-

235 fine our estimate using orbital and Yarkovsky clones of the real cluster members,
236 in a way similar to that proposed by Vokrouhlický and Nesvorný (2011).

237 3.1 *Orbital evolution of the cluster members*

238 In our first application of the BIM, only the orbits of real family members are
239 used to estimate the family age. In order to apply the BIM, two conditions must
240 be fulfilled: (1) the family must be young (up to about 10 Myr); and (2) the family
241 members must be dynamically stable. The first condition is nearly certainly satis-
242 fied based on the very tight packing of the Gibbs cluster members in the proper
243 orbital space as discussed in Section 2. The fulfillment of the second condition is
244 verified by calculating Lyapunov times (T_{lyap}) for all objects belonging to the clus-
245 ter. In practical terms, for the purpose of this study, objects are considered stable
246 if $T_{lyap} > 10^5$ yr. This condition is satisfied for all members of the cluster (see
247 Table 2).

248 The evolution of the average of the mean differences in the two secular angles, de-
249 rived from the numerical integration of the orbits of the cluster members, is shown
250 in Figure 3. The results clearly show a tight clustering (within 7 degrees) of both
251 angles at ~ 1.5 Myr in the past. This clustering very likely corresponds to the time
252 of family formation. Such a conclusion is additionally supported by the past evo-
253 lution of individual orbits of all 9 members of the cluster. As it is shown in Fig. 4,
254 both secular angles, the nodal longitudes and arguments of perihelion, were very
255 close at this time. Furthermore, the latter result also indicates that all 9 asteroids are
256 likely real members of the Gibbs cluster.

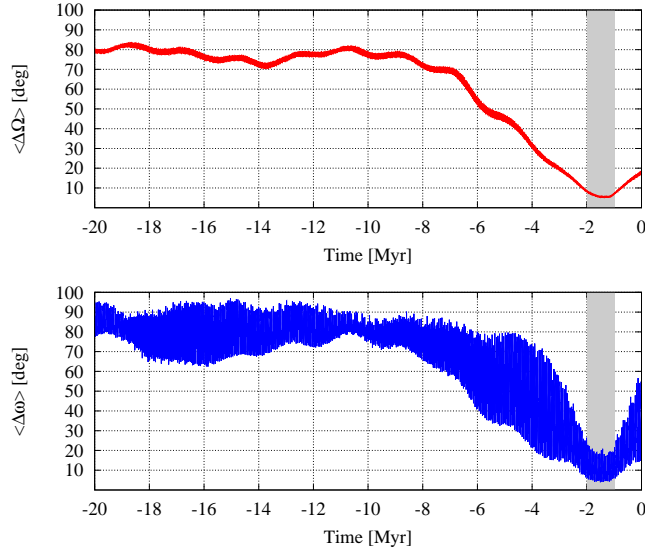


Fig. 3. The average of differences in the mean longitudes of the ascending nodes Ω (top), and arguments of perihelion ω (bottom), for the 9 nominal members of the Gibbs cluster. These results are obtained in a purely gravitational model. The most important feature (clearly visible in both plots) is a deep clustering of both angles occurring about 1.5 Myr in the past.

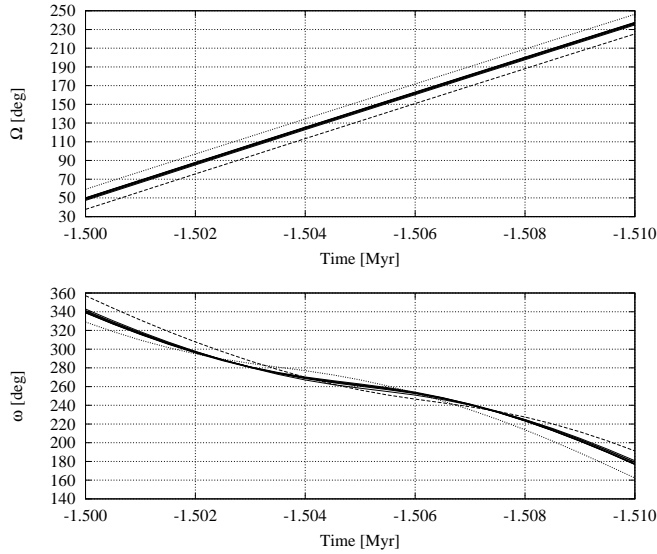


Fig. 4. The plot shows past orbital evolutions of nodal longitudes, Ω (top) and arguments of perihelion, ω (bottom) at about 1.5 Myr ago for all 9 members of the Gibbs cluster. At this time both angles of all 9 asteroids were nearly the same, suggesting that the cluster was created by a recent catastrophic collision.

257 3.2 *Orbital and Yarkovsky clones*

258 To further refine our BIM determination of the age of the cluster, we use a method-
259 ology first proposed by Nesvorný and Vokrouhlický (2006) and used in the past
260 to estimate the ages of some young clusters (e.g., Vokrouhlický and Nesvorný,
261 2011; Novaković et al., 2012b). Thus, we refer the reader to these papers for ad-
262 ditional information about the method. In principle, the BIM is affected by two
263 major sources of error. These are due on one hand to unavoidable uncertainties in
264 the orbital elements of known family members, and on the other hand to a well-
265 known secular evolution of the semi-major axis caused by the Yarkovsky thermal
266 force (Bottke et al., 2006). The latter depends, in turn, upon the thermal properties
267 of the objects’ surfaces and on the value of the obliquity angle. As a consequence
268 of the Yarkovsky mechanism, the semi-major axis can either increase or decrease
269 with time. In order to account for the above effects, we extend our analysis by
270 considering a large sample of synthetic clones.

271 For this analysis, we generate a set of statistically equivalent orbital and Yarkovsky
272 (hereafter ‘yarko’) clones. Specifically, for each nominal member of the Gibbs clus-
273 ter, we create 10 orbital clones, and for each of the orbital clones, we generate 10
274 different yarko clones corresponding to different possible drift rates of the orbital
275 semi-major axis. Orbital clones are generated using 3σ uncertainties of each clus-
276 ter member’s osculating orbital elements, assuming Gaussian distributions.² Yarko
277 clones are distributed randomly over the interval $\pm(da/dt)_{max}$, where $(da/dt)_{max}$

² A better way to produce orbital clones would be to use random distribution based on the full correlation matrix. The approach we used here makes clones somewhat more dispersed, resulting in slightly larger uncertainty of the age than necessary. Still, we used this method due to its simplicity.

278 is the maximum expected value of the semi-major axis drift speed caused by the
 279 Yarkovsky effect. This random da/dt distribution corresponds to an isotropic dis-
 280 tribution of spin axes. At the location of the Gibbs cluster, for a body of $D = 1$ km
 281 in diameter, we use a value of $(da/dt)_{max} = 4 \times 10^{-4}$ AU/Myr, which scales as
 282 $1/D$. This drift limit was determined assuming thermal and physical parameters
 283 appropriate for C-type asteroids (see e.g. Brož and Vokrouhlický, 2008). Note also
 284 that we only take into account the diurnal component of the Yarkovsky effect, be-
 285 cause the seasonal variant is negligible for the objects of these sizes (Bottke et al.,
 286 2006). In this way, we assign a total of 100 statistically equivalent clones to each
 287 real member of the cluster.

288 We then numerically integrate the orbits of all clones backward in time for 2 Myr
 289 using the *ORBIT9* software package (Milani and Nobili, 1988). The adopted dy-
 290 namical model includes four major planets, from Jupiter to Neptune, as perturbing
 291 bodies, and accounts for the Yarkovsky effect.

The age of the cluster is defined as the minimum of the function

$$\Delta V = na\sqrt{(\sin(i)\Delta\Omega)^2 + 0.5(e\Delta\varpi)^2} \quad (1)$$

292 where $na \approx 17.2$ km s⁻¹ is the mean orbital speed of the asteroids in the Gibbs clus-
 293 ter, and $\Delta\Omega$ and $\Delta\varpi$ are the dispersions of the longitude of node and the longitude
 294 of perihelion, respectively (Vokrouhlický and Nesvorný, 2011). We then obtain the
 295 final age of the cluster by performing 10^6 trials of this procedure, randomly se-
 296 lecting one clone of each member, and determining the minimum of the function
 297 defined above for all of the clone combinations.

298 The histogram of the ages we obtain using this method is shown in Figure 5. We
 299 find the age of the Gibbs cluster to be 1.5 ± 0.1 Myr.

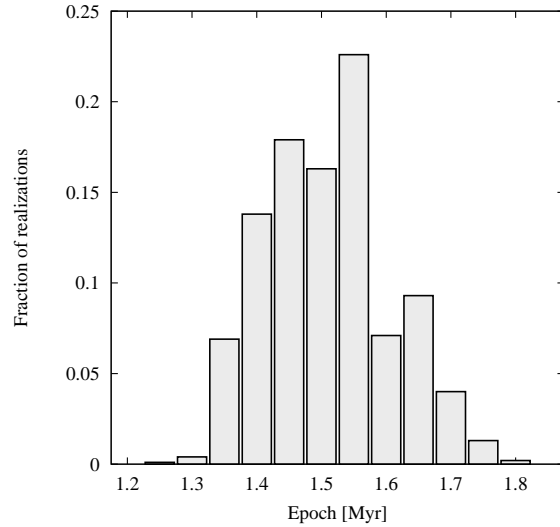


Fig. 5. Histogram of possible ages of the Gibbs cluster, produced using 10^6 different combinations of orbital and Yarkovsky clones.

300 **4 Physical properties of the Gibbs cluster**

301 Unfortunately, very little physical and spectral information about the members of
 302 the Gibbs cluster exists. The only data at our disposal come from SDSS spec-
 303 trophotometric observations and corresponding taxonomic classification. Specifi-
 304 cally, Gibbs cluster members (140429) 2001TQ₉₆ and (177075) 2003FR₃₆ are both
 305 classified as *Q*-class objects, although with probabilities of only 32% and 13% re-
 306 spectively (see Carvano et al., 2010, for more details on the classification). If these
 307 classifications are correct, we might expect all Gibbs cluster members to be *Q*-type
 308 asteroids since the members of an asteroid family tend to share similar spectral
 309 properties (e.g. Cellino et al., 2002).

310 This would be a very interesting result because *Q*-type asteroids are spectroscop-
 311 ically more similar to ordinary chondrite meteorites than any other asteroid class
 312 (Bus and Binzel, 2002), and it has been suggested that *Q*-class asteroids, which are
 313 most common among near-Earth objects (NEOs), have young surfaces. As a conse-
 314 quence, space weathering (SW; Gaffey, 2010; Marchi et al., 2012) has presumably

315 not had sufficient time to transform the surfaces of *Q*-class asteroids into those typi-
316 cal of classical and more common *S*-type asteroids. The timescale for an asteroid to
317 transition from *Q*-type to *S*-type is still not well understood. Cellino et al. (2010)
318 did not find differences in polarimetric properties of equal-sized members of the
319 Koronis and Karin families, implying that SW acts on timescales shorter than the
320 age of the Karin family, or about 6 Myr. Vernazza et al. (2009) claimed that SW
321 rapidly reddens asteroid surfaces in less than 1 Myr. However, this may be incon-
322 sistent with the observed fraction of *Q*-type asteroids among NEOs. To reconcile
323 this problem, Binzel et al. (2010) proposed that during close encounters between
324 NEOs and the Earth-Moon system, tidal forces could cause surface shaking that
325 rejuvenates the surface regolith of these objects, thus, returning them from *S*-types
326 back to *Q*-types. On the other hand, recent work by Nesvorný et al. (2010) suggests
327 a timescale longer than 1 Myr for SW to affect NEO spectra, so there may be no
328 conflict to resolve after all.

329 Interestingly, the first examples of main belt *Q*-type asteroids were found just re-
330 cently among the members of very young asteroid families (Mothé-Diniz and Nesvorný,
331 2008). In this respect, our findings for the Gibbs cluster could be interpreted as an
332 indication that, at these heliocentric distances, SW mechanisms require longer than
333 1.5 Myrs (our derived age of the family) to change the spectrophotometric proper-
334 ties of bodies having an overall composition similar to that of ordinary chondrites.
335 However, taxonomic classifications based on multi-band photometry covering only
336 a few color channels are obviously not as precise as classifications derived from full
337 reflectance spectra, and so therefore caution is required to avoid over-interpreting
338 the scarce data at our disposal.

339 We note that Rivkin et al. (2011) analyzed some members of the Koronis family
340 (about 1-2 billion years old) and found that *Q*-type asteroids are also present in the

341 main-belt among asteroids smaller than about 4 km (see also Thomas et al., 2011,
342 2012). These results are not necessarily at odds with our conclusions about possibly
343 young surfaces among Gibbs cluster members, but they do perhaps indicate that
344 more work is needed to better understand the nature of *Q*-type asteroids.

345 Other physical parameters can be derived for the members of the Gibbs cluster
346 based on their absolute magnitude values taken from catalogs, and making assump-
347 tions about albedo and composition. Given the uncertainties on the few available
348 spectrophotometric data, we decided to assume two different values for the geo-
349 metric albedo p_v and the density ρ , assuming two possible physical situations. As
350 such, we consider the case of primitive *C*-type objects having low albedo and den-
351 sity ($p_v = 0.05$ and $\rho = 1.3 \text{ g cm}^{-3}$) and the case of *S*-type asteroids with higher
352 albedos and densities ($p_v = 0.2$ and $\rho = 2.5 \text{ g cm}^{-3}$) (Carry, 2012).

353 First, for both sets of physical parameters, we compute the diameters of all cluster
354 members using the absolute magnitudes provided by the *AstDyS* website. These
355 results are also given in Table 2. It should be noted that the largest member, aster-
356 oid (20674) 1999 VT₁, is significantly larger than all other members, about 3 times
357 larger than the second largest member, asteroid (140429) 2001 TQ₉₆. This situation
358 is unlikely to be the consequence of observational incompleteness because all as-
359 teroids with $H < 15$ at heliocentric distances of ~ 3 AU are believed to have been
360 discovered (Gladman et al., 2009).

361 Next, we estimate a lower limit for the diameter of the parent body D_{PB} (assuming
362 a spherical shape) by summing-up the volumes of all known members. We find that
363 $D_{PB} \geq 18.3 \text{ km}$ or $D_{PB} \geq 9.1 \text{ km}$, depending on the albedos assumed for cluster
364 members. Corresponding escape velocities are $\sim 7.8 \text{ m s}^{-1}$ or $\sim 5.4 \text{ m s}^{-1}$, respec-
365 tively for the two cases, taking into account the assumed density values mentioned

366 above. We also note that if we follow the arguments developed by Tanga et al.
367 (1999), the parent body’s diameter could not have been less than the sum of the
368 sizes of the two largest members. The resulting parent body size turns out therefore
369 to be on about 24 km (assuming $p_V = 0.05$) or about 12 km (assuming $p_V = 0.2$).

370 As we have already noted, asteroid 20674 is by far the largest member of the
371 Gibbs cluster. The mass ratio between the largest fragment and the parent body
372 is $M_{LF}/M_{PB} \approx 0.9$. Based on these findings, the collision producing the Gibbs
373 cluster should be considered to be between a catastrophic disruption and a crater-
374 ing event. Additional information, such as the discovery of more cluster members
375 or better observational data for the cluster members, is certainly needed to better
376 constrain the nature of the initial family-forming fragmentation event.

377 **5 The observations**

378 *5.1 Search for new main-belt comets*

379 Young asteroid families located in the outer regions of the asteroid main belt are
380 thought to be the best candidates to look for new main-belt comets (Hsieh, 2009).
381 For these reasons, we have carried out observations of 5 members of the Gibbs
382 cluster and of 2 additional nearby background objects.

383 From the observational point of view, the major difficulty in identifying new MBCs
384 is that of being able to detect their elusive cometary-like activity that is both weak
385 and transient. Several techniques to attack this problem have been used so far (see
386 Hsieh, 2009; Sonnett et al., 2011; Waszczak et al., 2013, and references therein).

387 The approach that we followed here includes optical imaging and adopts two dif-

388 ferent search methods. The first method is based on the so-called Stellarity Index,
389 derived from SExtractor (Bertin and Arnouts, 1996). This is designed to discrim-
390 inate between the images of point-like and extended sources. The second method
391 consists in comparing surface brightness profiles of both the target and a nearby
392 reference star (Hsieh and Jewitt, 2005). A possible excess in an asteroid’s profile,
393 would be diagnostic of the presence of a comet-like coma.

394 We obtained *R*-band imaging of seven targets using the Imager/Low Resolution
395 Spectrograph Do.Lo.Res of the 3.6 m Telescopio Nazionale Galileo (TNG) located
396 at the Observatorio del Roque de los Muchachos (ORM) at La Palma, Canary Is-
397 lands. Do.Lo.Res (Device Optimized for the Low Resolution) is a focal reducer
398 instrument installed at the Nasmyth B focus of the TNG. The detector is a 2048 ×
399 2048 E2V 4240 thinned back-illuminated, deep-depleted, Astro-Broadband coated
400 CCD with a pixel size of 13.5 μ . The plate scale is 0''.252 pixel⁻¹, yielding a field
401 of view of about 8.6' × 8.6'. Observations were carried out in service/queue mode
402 between August 2012 and January 2013. Observational circumstances are listed in
403 Table 3.

404 All the observing nights were photometric, with sub-arcsecond seeing. Seeing data
405 were available in real-time from the TNG DIMM and extinction data in the SDSS *r*
406 band were available from the webpage of the Carlsberg Meridian Circle telescope
407 at the ORM. For all targets, the same observation sequence was adopted of 12 ex-
408 posures of 300 s each (total integration time of 3600 s) while tracking each asteroid
409 with its proper differential motion. During each night, a photometric standard star
410 field (Landolt, 1992) was observed to derive the average zero-point. We estimate the
411 errors of the photometric calibration of the fields to be 0.03 mag or less for all fields.
412 Images were reduced following standard procedures using IRAF routines. First, a
413 master bias frame was created for each night by averaging all bias frames obtained

Table 3

Observational circumstances of the 7 targets observed at the TNG. All observations were obtained using *R*-Johnson filter.

UT date ^a	UT time ^b	Target ^c	Ext. ^d	DIMM ^e	t ^f	R ^g	Δ ^h	ν ⁱ
17/08/2012	2.5579	2002 TF ₃₂₅	0.147	0.75	3600	3.001	1.999	271.4
17/08/2012	3.8192	2007 RT ₁₃₈	0.147	0.75	3600	2.989	2.019	278.8
19/09/2012	1.5640	16290	0.129	0.85	3600	2.851	2.123	34.2
19/09/2012	2.9158	82522	0.129	0.85	3600	2.889	2.206	37.9
25/09/2012	4.3553	140429	0.171	0.90	3600	2.875	2.693	40.9
12/01/2013	4.1661	177075	0.087	0.75	3600	3.025	2.283	107.8
12/01/2013	5.5408	249738	0.087	0.75	3600	3.030	2.358	109.9

^a Date of the observation

^b Universal time of the observation in hrs

^c Asteroid (target) number or provisional designation

^d Extinction in mag/airmass

^e Differential Image Motion Monitor seeing in arcsec

^f Total integration time in sec

^g Heliocentric distance in AU

^h Geocentric distance in AU

ⁱ True anomaly in degrees

414 that night. All images were then bias-corrected by subtracting the corresponding
 415 master bias. A master flat-field frame was obtained by averaging the bias-corrected
 416 flat-field images and normalizing to the median intensity value. Images were then
 417 corrected for pixel-to-pixel response variations dividing by the corresponding flat-
 418 field frames. Given the non-negligible apparent differential motion of the asteroids
 419 with respect to the background star field, a suitable non-zero differential R.A./Dec.

420 tracking rate was applied to the telescope TCS for each target. This produces a field
421 where only the asteroid is a point-like source while all the other sources are trailed.
422 The final 3600 s image of each asteroid was obtained by aligning, registering and
423 stacking each 300 s image to the position of the asteroid on the CCD corresponding
424 as measured in the 6th image (i.e. the middle of the acquisition sequence).

425 The next step is to check for possible signs of cometary activity of the observed
426 objects. Our first approach utilizes SExtractor (Bertin and Arnouts, 1996), a soft-
427 ware package developed to detect, measure and classify sources from astronomical
428 images. Having been originally designed to distinguish between stars and galaxies,
429 it allows users to discriminate between point-like and extended objects.

430 We use SExtractor to derive all the photometric/morphological parameters such as
431 flux, background level, R -band magnitude, FWHM, ellipticity and Stellerity Index
432 (SI). These results are shown in Table 4.

433 In particular, the latter parameter has been used to discriminate between point-like
434 and extended sources. This parameter is the result of a supervised trained neu-
435 ral network to perform star-galaxy classification. In theory, SExtractor considers
436 objects with $SI=0.0$ to be galaxies and those with $SI=1.0$ to be stars. In practice,
437 objects are classified as stars by selecting $SI \geq 0.9$. Since the SI depends on the as-
438 sumed FWHM of the stars in the image and the 3600 s exposures of our targets only
439 have the target itself as the sole non trailed source, we also acquired a short 20 s
440 exposure of each field so that the differential tracking rate would not produce any
441 smearing of the stars and derived the average FWHM from that image. We take into
442 account any fluctuation of the seeing during the 12×300 s sequence by checking the
443 DIMM seeing. Despite a differential tracking rate was applied to the TCS we found
444 that 4 out of 7 targets do have a quite elongated PSF (ellipticity values between

Table 4

Photometric Data for our 7 target asteroids. The R -band magnitude of each object is shown, as well as the 5σ detection limit magnitude for point-like and extended sources in each frame. Stellerity Indices are reported to discriminate between point-like and extended objects.

Target	FWHM ^a	m_R ^b	Limit mag 1 ^c	Limit mag 2 ^d	SI ^e
2002 TF ₃₂₅	0.92	21.13	24.61	25.14	0.98
2007 RT ₁₃₈	0.88	19.70	24.60	25.08	0.98
16290	1.21	19.12	24.12	24.95	0.97
82522	1.09	18.57	24.44	25.16	0.99
140429	1.40	20.37	23.69	24.67	0.98
177075	0.93	20.31	24.67	25.21	0.98
249738	0.99	20.70	24.40	25.01	0.98

^a FWHM in arcsec

^b R -band apparent magnitude

^c 5σ R -band detection limit magnitude for point-like sources

^d 5σ R -band detection limit magnitude for extended sources in mag/arcsec²

^e SExtractor Stellerity Index

445 0.110 and 0.155). However, we attribute this elongation most likely to the presence
 446 of aberrations in the telescope optics, since no Shack-Hartman analysis was per-
 447 formed before observations. This is why we adopted a flexible elliptical aperture
 448 (Kron, 1980) instead of a simple circular aperture for photometry. Moreover, this is
 449 the best choice when any object could have a intrinsic diffused/elongated structure.
 450 All our targets are found to have SI values of ≥ 0.97 . As a result, we conclude that
 451 none of the asteroids observed in our program show any evidence of cometary-like
 452 activity.

453 To confirm the above conclusions based on the Stellerity Index, we also analyze
454 all obtained images by comparing surface brightness profiles of each asteroid and a
455 corresponding reference star. This technique is best suited for detecting coma that
456 extends radially in all directions from an object, or directed emission not aligned
457 with the direction of the object's apparent motion. It cannot be used to detect emis-
458 sion oriented along the direction of an object's apparent motion.

459 We combine individual images of each object into a single high signal-to-noise
460 ratio composite image to search for any features that would indicate comet-like ac-
461 tivity. In each case, images are shifted and aligned on corresponding object's pho-
462 tocenter using a fifth-order polynomial interpolation and averaged. As was found
463 by Hsieh and Jewitt (2005), this process produces less noisy profiles than median
464 combination. Additionally, all images are shifted and aligned on the photocenter of
465 a nearby reference field star. We can then obtain one-dimensional surface bright-
466 ness profiles by averaging over horizontal rows over the entire widths of the object
467 and reference star, and by subtracting sky background sampled from either side of
468 the object or star. These profiles are then normalized to unity and shown together in
469 Figure 6 to search for dissimilarities. Specifically, we looked for excess flux in each
470 asteroid's profile that would imply the presence of a coma. By analyzing Figure 6,
471 we note that some scatter is present in the wings of some of the asteroid profiles, but
472 we attribute this to low signal-to-noise ratios far from the nucleus. Thus, we con-
473 clude that no coma is found, in agreement with results we obtained using method
474 based on the SExtractor.

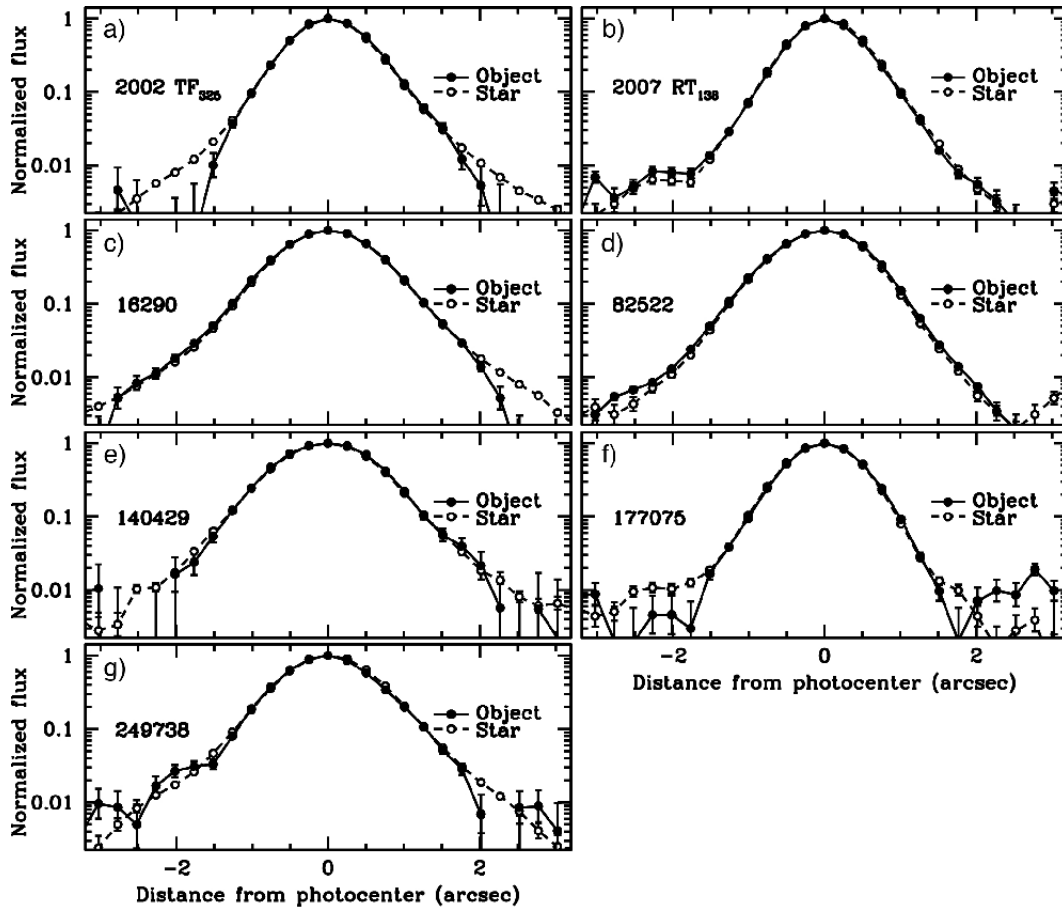


Fig. 6. Comparison of the surface brightness profiles of the composite images of observed asteroids and corresponding reference stars. Surface brightness is normalized to unity at each profiles peak and is plotted on a logarithmic scale against angular distance in the plane of the sky.

475 5.2 Observations of P/2012 F5 Gibbs

476 We also obtained 8 *R*-band images totalling 4080 s of effective exposure time on
 477 UT 2013 May 12, and 6 *R*-band images totalling 1800 s of effective exposure time
 478 on UT 2013 May 13 of P/2012 F5 using the University of Hawaii (UH) 2.2 m tele-
 479 scope on Mauna Kea. Obtained under photometric conditions, these observations
 480 utilized a Tektronix 2048×2048 pixel CCD with an image scale of $0''.219 \text{ pixel}^{-1}$
 481 and a Kron-Cousins *R*-band filter. Standard bias subtraction and flat-field reduction

482 were performed on all images, where flat fields were constructed from dithered
483 images of the twilight sky. Photometry of Landolt (1992) standard stars was ob-
484 tained by measuring net fluxes (over sky background) within circular apertures,
485 with background sampled from surrounding circular annuli. Asteroid photometry
486 was performed similarly, except that to avoid the contaminating effects of any near-
487 nucleus dust, background sky statistics were measured manually in regions of blank
488 sky near, but not adjacent, to the object. Several (5-10) field stars in the object im-
489 ages were also measured and used to correct for minor extinction variation during
490 each night.

491 We use these observations to estimate the absolute magnitude of P/2012 F5, finding
492 $H_R \approx 17.0 \pm 0.1$ mag and $H_V \approx 17.4 \pm 0.1$ mag in R - and V -band respectively,
493 assuming $G = 0.15$ for both filters. While the object appears point-source-like in
494 these images, very large dust grains ejected during P/2012 F5's original outburst
495 event in 2012 could have a dissipation rate from the nucleus that is slow enough
496 that they had not yet drifted beyond the seeing disk of the nucleus at the time of our
497 observations. If this is the case, their additional scattering surface area could have
498 contributed to the total flux observed from the nucleus, even though no observable
499 evidence of residual activity (either in the form of visible coma or a non-stellar
500 PSF) was present. As such, we cannot absolutely rule out the presence of unre-
501 solved large dust grains in the seeing disk of the nucleus. Based on these absolute
502 magnitude limits, we set an upper limit on the diameter of the nucleus of ~ 2 km
503 (see Table 2).

504 **6 Discussions and Conclusions**

505 Our discovery of a young cluster associated with P/2012 F5 opens many different
506 opportunities for future work. In this respect, three characteristics of the cluster are
507 of particular importance. First, it is extremely compact in proper orbital elements,
508 and its statistical significance is very high, meaning that its members are very likely
509 to be fragments originating from a common parent body. Second, the Gibbs cluster
510 is very young, being only about 1.5 Myr old. Third, it is located in a dynamically
511 cold region of the main-belt, and thus its post-impact evolution is bounded. The
512 study of young and well preserved families like the Gibbs cluster are essential for
513 studies of impact physics, space weathering effects, and dynamical evolution.

514 In terms of studying space weathering, it is clear that the Gibbs cluster deserves fur-
515 ther observations in the near future. In particular, we encourage observations aimed
516 at developing better physical characterizations of the members of the Gibbs clus-
517 ter, either via broadband photometry or spectroscopy. In this regard, high quality
518 reflectance spectroscopy of the largest member, asteroid (20674) 1999 VT₁, would
519 be extremely valuable. A good opportunity to obtain such spectroscopy will be in
520 September 2014, during the asteroid's next opposition.

521 Currently available SDSS data for two Gibbs cluster members suggest that 1.5 Myr
522 is an insufficient length of time at these heliocentric distances to transform ordinary
523 achondrite spectra into more typical *S*-type spectra. As we have already cautioned
524 though, these conclusions are based on uncertain data and should be considered pre-
525 liminary. Fortunately, uncertainties in the physical properties of the cluster mem-
526 bers has only limited influence our determination of the age of the cluster. However,
527 as the physical properties of the cluster affect our estimates of the size of the par-

528 ent body, better physical characterizations of cluster members would certainly be
529 useful for refining our understanding of the initial family forming event.

530 As explained in Section 5, we were unsuccessful in our attempts to detect comet-
531 like activity among other members of the Gibbs cluster. This can be interpreted
532 either as a consequence of the fact that some faint activity could actually be present,
533 but it was below the detection limits of our observations. The other possibility is
534 that activity was actually absent, at least at the times when our observations were
535 carried out. Activity is known to be transient even for currently active MBCs (e.g.,
536 Hsieh et al., 2010, 2011), and only three of our targets were observed within the
537 approximate true anomaly range ($-50^\circ \lesssim \nu \lesssim 90^\circ$; i.e., close to and following
538 perihelion) where other MBCs have shown activity in the past (Hsieh et al., 2012).

539 However, perhaps the most important issues to keep in mind when interpreting
540 the lack of any detected activity in our observations of fellow cluster members of
541 P/2012 F5, is their composition as well as the active nature of P/2012 F5 itself. The
542 MBCs are expected to be low-albedo, icy-bearing objects, with spectra most closely
543 resembling that of *C*-type asteroids. If it turns out that the Gibbs cluster is indeed
544 composed of *Q*-type objects, as suggested by SDSS data, this would explain why
545 we did not find any activity in these asteroids. This hypothesis is supported by the
546 studies by Stevenson et al. (2012) and Moreno et al. (2012) who found that P/2012
547 F5's activity was most likely due to an impact from another asteroid and not comet-
548 like sublimation of volatile ices.

549 Thus, while we did not successfully detect any new comet among the Gibbs cluster,
550 this result does not necessarily invalidate the hypothesis that young asteroid fami-
551 lies and main-belt comets are linked, as there are several plausible explanations for
552 why no activity was detected. In fact, if P/2012 F5's activity was due to an impact

553 and not sublimation, making it a disrupted asteroid and not a comet, we perhaps
554 would not even expect to find other similar instances of comet-like activity given
555 the low likelihood of impacts in the asteroid belt, even in families as young as the
556 Gibbs cluster. As such, while the Gibbs cluster will certainly be an interesting sub-
557 ject for further studies of space weathering and catastrophic collisions in the main
558 asteroid belt, confirmation of the hypothesized link between young families and
559 main-belt comets will likely have to come from elsewhere.

560 **Acknowledgments**

561 We would like to express our gratitude to Mira Brož and Ricardo Gil-Hutton, the
562 referees, for the useful comments and suggestions which helped us to improve this
563 article. The work of B.N. has been supported by the Ministry of Education and Sci-
564 ence of Serbia under the Project 176011, and , in part, by the European Science
565 Foundation under the GREAT ESF RNP programme (Exchange Grant No. 3535).
566 H.H.H. is supported by NASA through Hubble Fellowship grant HF-51274.01
567 awarded by the Space Telescope Science Institute, which is operated by the As-
568 sociation of Universities for Research in Astronomy (AURA) for NASA, under
569 contract NAS 5-26555. Based in part on observations made with the Italian Tele-
570 scopio Nazionale Galileo (TNG) operated on the island of La Palma by the Fun-
571 dacin Galileo Galilei of the INAF (Istituto Nazionale di Astrofisica) at the Spanish
572 Observatorio del Roque de los Muchachos of the Instituto de Astrofisica de Ca-
573 narias. Based in part on observations with the University of Hawaii 2.2 m telescope
574 at Mauna Kea Observatory, Institute for Astronomy, University of Hawaii.

575 **References**

- 576 Bertin, E., Arnouts, S. 1996. SExtractor: Software for source extraction.. *Astron-*
577 *omy and Astrophysics Supplement Series* 117, 393-404.
- 578 Binzel, R. P., Morbidelli, A., Merouane, S., DeMeo, F. E., Birlan, M., Vernazza, P.,
579 Thomas, C. A., Rivkin, A. S., Bus, S. J., Tokunaga, A. T. 2010. Earth encounters
580 as the origin of fresh surfaces on near-Earth asteroids. *Nature* 463, 331-334.
- 581 Bottke, W. F., Jr., Vokrouhlický, D., Rubincam, D. P., Nesvorný, D. 2006. The
582 Yarkovsky and Yorp Effects: Implications for Asteroid Dynamics. *Annual Re-*
583 *view of Earth and Planetary Sciences* 34, 157-191.
- 584 Briani, G., Morbidelli, A., Gounelle, M., Nesvorný, D. 2011. Evidence for an
585 asteroid-comet continuum from simulations of carbonaceous microxenolith dy-
586 namical evolution. *Meteoritics and Planetary Science* 46, 1863-1877.
- 587 Brož, M., Vokrouhlický, D. 2008. Asteroid families in the first-order resonances
588 with Jupiter. *Monthly Notices of the Royal Astronomical Society* 390, 715-732.
- 589 Brož, M., Morbidelli, A. 2013. The Eos family halo. *Icarus* 223, 844-849.
- 590 Bus, S. J., Binzel, R. P. 2002. Phase II of the Small Main-Belt Asteroid Spectro-
591 scopic SurveyA Feature-Based Taxonomy. *Icarus* 158, 146-177.
- 592 Capria, M. T., Marchi, S., de Sanctis, M. C., Coradini, A., Ammannito, E. 2012.
593 The activity of main belt comets. *Astronomy and Astrophysics* 537, A71.
- 594 Carry, B. 2012. Density of asteroids. *Planetary and Space Science* 73, 98-118.
- 595 Carvano, J. M., Hasselmann, P. H., Lazzaro, D., Mothé-Diniz, T. 2010. SDSS-based
596 taxonomic classification and orbital distribution of main belt asteroids. *Astron-*
597 *omy and Astrophysics* 510, A43.
- 598 Cellino, A., Bus, S. J., Doressoundiram, A., Lazzaro, D. 2002. Spectroscopic Prop-
599 erties of Asteroid Families. *Asteroids III* (W.F. Bottke, A. Cellino, P. Paolicchi,
600 R.P. Binzel, Eds.), Univ. of Arizona Press, Tucson, pp.633-643.

601 Cellino, A., Dell’Oro, A. 2010. Asteroid Dynamical Families. Lecture Notes in
602 Physics, Berlin Springer Verlag 790, 137-193.

603 Cellino, A., Delbò, M., Bendjoya, P., Tedesco, E. F. 2010. Polarimetric evidence of
604 close similarity between members of the Karin and Koronis dynamical families.
605 Icarus 209, 556-563.

606 Dell’Oro, A., Paolicchi, P., Cellino, A., Zappalà, V. 2002. Collisional Rates within
607 Newly Formed Asteroid Families. Icarus 156, 191-201.

608 Gaffey, M. J. 2010. Space weathering and the interpretation of asteroid reflectance
609 spectra. Icarus 209, 564-574.

610 Gibbs, A. R., and 16 colleagues 2012. Comet P/2012 F5 (Gibbs). Central Bureau
611 Electronic Telegrams 3069, 1.

612 Gladman, B. J., and 11 colleagues 2009. On the asteroid belt’s orbital and size
613 distribution. Icarus 202, 104-118.

614 Gounelle, M., Morbidelli, A., Bland, P. A., Spurny, P., Young, E. D., Sephton, M.
615 2008. Meteorites from the Outer Solar System?. The Solar System Beyond Nep-
616 tune 525-541.

617 Hsieh, H. H. 2009. The Hawaii trails project: comet-hunting in the main asteroid
618 belt. Astronomy and Astrophysics 505, 1297-1310.

619 Hsieh, H. H., Jewitt, D. 2005. Search for Activity in 3200 Phaethon. The Astro-
620 physical Journal 624, 1093-1096.

621 Hsieh, H. H., Jewitt, D. 2006. A Population of Comets in the Main Asteroid Belt.
622 Science 312, 561-563.

623 Hsieh, H. H., Jewitt, D., Lacerda, P., Lowry, S. C., Snodgrass, C. 2010. The return
624 of activity in main-belt comet 133P/Elst-Pizarro. MNRAS 403, 363-377.

625 Hsieh, H. H., Meech, K. J., Pittichová, J. 2011. Main-Belt Comet 238P/Read Re-
626 visited. The Astrophysical Journal Letters 736, L18.

627 Hsieh, H. H., et al. 2012. Observational and dynamical characterization of main-

628 belt comet P/2010 R2 (La Sagra). *The Astronomical Journal* 143, 104.

629 Jewitt, D. 2012. The Active Asteroids. *The Astronomical Journal* 143, 66.

630 Kron, R. G. 1980. Photometry of a complete sample of faint galaxies. *The Astro-*
631 *physical Journal Supplement Series* 43, 305-325.

632 Landolt, A. U. 1992. UBVRI photometric standard stars in the magnitude range
633 11.5-16.0 around the celestial equator. *The Astronomical Journal* 104, 340-371.

634 Marchi, S., Paolicchi, P., Richardson, D. C. 2012. Collisional evolution and reddening
635 of asteroid surfaces - I. The problem of conflicting time-scales and the role
636 of size-dependent effects. *Monthly Notices of the Royal Astronomical Society*
637 421, 2-8.

638 Milani, A., Nobili, A. M. 1988. Integration error over very long time spans. *Celestial*
639 *Mechanics* 43, 1-34.

640 Milani, A., Knežević, Z. 1990. Secular perturbation theory and computation of as-
641 teroid proper elements. *Celest. Mech. Dynam. Astron.* 49, 347-411.

642 Milani, A., Knežević, Z. 1994. Asteroid proper elements and the dynamical struc-
643 ture of the asteroid main belt. *Icarus* 107, 219-254.

644 Morbidelli, A., Zappala, V., Moons, M., Cellino, A., Gonczi, R. 1995. Asteroid
645 families close to mean motion resonances: dynamical effects and physical impli-
646 cations. *Icarus* 118, 132.

647 Moreno, F., Licandro, J., Cabrera-Lavers, A. 2012. A Short-duration Event as the
648 Cause of Dust Ejection from Main-Belt Comet P/2012 F5 (Gibbs). *The Astro-*
649 *physical Journal* 761, L12.

650 Mothé-Diniz, T., Nesvorný, D. 2008. Visible spectroscopy of extremely young as-
651 teroid families. *Astronomy and Astrophysics* 486, L9-L12.

652 Nesvorný, D., Bottke, W. F., Jr., Dones, L., Levison, H. F. 2002. The recent breakup
653 of an asteroid in the main-belt region. *Nature* 417, 720-771.

654 Nesvorný, D., Bottke, W. F., Levison, H. F., Dones, L. 2003. Recent Origin of the

655 Solar System Dust Bands. *The Astrophysical Journal* 591, 486-497.

656 Nesvorný, D., Vokrouhlický, D. 2006. New Candidates for Recent Asteroid
657 Breakups. *The Astronomical Journal* 132, 1950-1958.

658 Nesvorný, D., Vokrouhlický, D., Bottke, W. F. 2006. The Breakup of a Main-Belt
659 Asteroid 450 Thousand Years Ago. *Science* 312, 1490.

660 Nesvorný, D., Bottke, W. F., Vokrouhlický, D., Sykes, M., Lien, D. J., Stansberry,
661 J. 2008. Origin of the Near-Ecliptic Circumsolar Dust Band. *The Astrophysical*
662 *Journal* 679, L143-L146.

663 Nesvorný, D., Bottke, W. F., Vokrouhlický, D., Chapman, C. R., Rafkin, S. 2010.
664 Do planetary encounters reset surfaces of near Earth asteroids?. *Icarus* 209, 510-
665 519.

666 Novaković, B., Tsiganis, K., Knežević, Z. 2010. Chaotic transport and chronology
667 of complex asteroid families. *Monthly Notices of the Royal Astronomical Soci-*
668 *ety* 402, 1263-1272.

669 Novaković, B. 2010. Portrait of Theobalda as a young asteroid family. *Monthly*
670 *Notices of the Royal Astronomical Society* 407, 1477-1486.

671 Novaković, B., Cellino, A., Knežević, Z. 2011. Families among high-inclination
672 asteroids. *Icarus* 216, 69-81.

673 Novaković, B., Hsieh, H. H., Cellino, A. 2012a. P/2006 VW₁₃₉: a main-belt comet
674 born in an asteroid collision? *Monthly Notices of the Royal Astronomical Soci-*
675 *ety* 424, 1432-1441.

676 Novaković, B., Dell'Oro, A., Cellino, A., Knežević, Z. 2012b. Recent collisional jet
677 from a primitive asteroid. *Monthly Notices of the Royal Astronomical Society*
678 425, 338-346.

679 Pravec, P., Vokrouhlický, D. 2009. Significance analysis of asteroid pairs. *Icarus*
680 204, 580-588.

681 Rivkin, A. S., Thomas, C. A., Trilling, D. E., Enga, M.-T., Grier, J. A. 2011. Ordi-

682 nary chondrite-like colors in small Koronis family members. *Icarus* 211, 1294-
683 1297.

684 Sonnett, S., Kleyana, J., Jedicke, R., Masiero, J. 2011. Limits on the size and orbit
685 distribution of main belt comets. *Icarus* 215, 534-546.

686 Stevenson, R., Kramer, E. A., Bauer, J. M., Masiero, J. R., Mainzer, A. K. 2012.
687 Characterization of Active Main Belt Object P/2012 F5 (Gibbs): A Possible Im-
688 pacted Asteroid. *The Astrophysical Journal* 759, 142

689 Takato, N. 2008. Rotation-Resolved Spectroscopy of a Very Young Asteroid,
690 (1270) Datura. *The Astrophysical Journal* 685, L161-L163.

691 Tanga, P., Cellino, A., Michel, P., Zappalà, V., Paolicchi, P., Dell’Oro, A. 1999. On
692 the Size Distribution of Asteroid Families: The Role of Geometry. *Icarus* 141,
693 65.

694 Thomas, C. A., Rivkin, A. S., Trilling, D. E., Marie-Therese Enga, Grier, J. A.
695 2011. Space weathering of small Koronis family members. *Icarus* 212, 158-166.

696 Thomas, C. A., Trilling, D. E., Rivkin, A. S. 2012. Space weathering of small Ko-
697 ronis family asteroids in the SDSS Moving Object Catalog. *Icarus* 219, 505-507.

698 Vernazza, P., Birlan, M., Rossi, A., Dotto, E., Nesvorný, D., Brunetto, R., Fornasier,
699 S., Fulchignoni, M., Renner, S. 2006. Physical characterization of the Karin fam-
700 ily. *Astronomy and Astrophysics* 460, 945-951.

701 Vernazza, P., Binzel, R. P., Rossi, A., Fulchignoni, M., Birlan, M. 2009. Solar wind
702 as the origin of rapid reddening of asteroid surfaces. *Nature* 458, 993-995.

703 Vokrouhlický, D., Brož, M., Morbidelli, A., Bottke, W. F., Nesvorný, D., Lazzaro,
704 D., Rivkin, A. S. 2006. Yarkovsky footprints in the Eos family. *Icarus* 182, 92-
705 117.

706 Vokrouhlický, D., and 12 colleagues 2009. Datura family: the 2009 update. *Astron-
707 omy and Astrophysics* 507, 495-504.

708 Vokrouhlický, D., Nesvorný, D. 2011. Half-brothers in the Schulhof Family?. *The*

709 Astronomical Journal 142, 26.

710 Willman, M., Jedicke, R., Moskovitz, N., Nesvorný, D., Vokrouhlický, D., Mothé-
711 Diniz, T. 2010. Using the youngest asteroid clusters to constrain the space weath-
712 ering and gardening rate on S-complex asteroids. *Icarus* 208, 758-772.

713 Waszczak, A., and 10 colleagues 2013. Main-belt comets in the Palomar Transient
714 Factory survey - I. The search for extendedness. *Monthly Notices of the Royal*
715 *Astronomical Society* 433, 3115-3132.

716 Zappalà, V., Cellino, A., Farinella, P., Knežević, Z. 1990. Asteroid families. I - Iden-
717 tification by hierarchical clustering and reliability assessment. *The Astronomical*
718 *Journal* 100, 2030-2046.

719 Zappalà, V., Cellino, A., Farinella, P., Milani, A. 1994. Asteroid families. 2: Exten-
720 sion to unnumbered multiopposition asteroids. *The Astronomical Journal* 107,
721 772-801.

722 Zappalà, V., Cellino, A., Dell'Oro, A., Paolicchi, P. 2002. Physical and Dynam-
723 ical Properties of Asteroid Families. *Asteroids III* (W.F. Bottke, A. Cellino, P.
724 Paolicchi, R.P. Binzel, Eds.), Univ. of Arizona Press, Tucson, pp.619-631.

725 Ziffer, J., Campins, H., Licandro, J., Walker, M. E., Fernandez, Y., Clark, B. E.,
726 Mothe-Diniz, T., Howell, E., Deshpande, R. 2011. Near-infrared spectroscopy
727 of primitive asteroid families. *Icarus* 213, 538-546.